DINAME 2023 - Proceedings of the XIX International Symposium on Dynamic Problems of Mechanics,
A.S. De Paula, A.T. Fabro and M.R. Machado (Editors), ABCM.
Pirenópolis, Go, Brazil, February 26th to March 3rd, 2023

Chaos Control in a Nonlinear Pendulum Using a Generalized Extended Time-Delayed Feedback Method

Arthur Rodrigues Queiroz[1], **Aline Souza de Paula**[1], **Marcelo A. Savi**[2]

[1] Universidade de Brasília, Campus Universitário Darcy Ribeiro, Brasília-DF - CEP 70910-900

[2] Universidade Federal do Rio de Janeiro, COPPE - Mechanical Engineering, Center for Nonlinear Mechanics

Abstract: Chaos control is based on the stabilization of unstable periodic orbits (UPOs) embedded in chaotic behavior by means of tiny disturbances. The Extended Time-Delayed Feedback Control Method is a continuous approach associated with a scalar gain. This paper considers a generalization of the method, assuming a matrix controller gain instead of a scalar, investigating its influence on the control efficacy. The control performance for different gains is compared in terms of stabilization time and maximum control perturbation. A case study of a nonlinear pendulum is of concern, which consists of a metallic disk with eccentrically concentrated mass, excited by a motor-spring-wire system. Lyapunov exponents of the UPOs are employed as controller parameter criterion. Results show that matrix gain increases the controlability when compared with the scalar gain.

Keywords: Chaos control, nonlinear dynamics, pendulum, ETDF.

INTRODUCTION

Natural phenomena are full of nonlinearities where chaotic behavior is one of the possibilities with an intrinsic richness. The chaotic behavior has a strong dependence of initial conditions, which makes small perturbations to produce huge, disproportional effects. Besides, chaos has a dense and infinite set of unstable periodic orbits (UPOs). This richness makes chaos of special interest in dynamical system design, conferring flexibility that can be observed by quick changes among different kinds of responses.

Chaos control takes advantage of these essential characteristics of chaotic behavior, stabilizing a specific UPO by tiny perturbations. Chaos control may be divided into two stages: the learning stage, where UPOs are identified and the controller parameters are evaluated; and the stabilization stage, where perturbations are employed to stabilize the desired UPOs.

Chaos control methods may be classified as continuous or discrete. Historically, the OGY (Ott-Grebogi-Yorke) method Ott *et al.* (1990) is the pioneer work related to the a discrete method that promotes the stabilization forcing the system to stay at the stable manifold from perturbations in a controller parameter applied in a Poincaré section. Several improvements of this method were developed in the literature (De Paula and Savi, 2011). On the other hand, continuous methods tend to be more robust increasing the number of perturbations. The first method applying this idea was the time-delayed feedback (TDF) control proposed by Pyragas (1992) where an UPO is stabilized by a continuous feedback perturbation proportional to the difference between the present and the delayed state of the system. An improvement of TDF control is the Extended Time-Delayed Feedback (ETDF) control which uses several delayed states of the system instead of one (Socolar *et al.*, 1994). Other improvements consider variable delays, (Jüngling *et al.*, 2012), the modulation of the delays (Gjurchinovski *et al.*, 2013), and adaptive tuning of delay time (Pyragas and Pyragas, 2011, 2013; Selivanov *et al.*, 2015).

Continuous methods are presented in a wide range of applications. TDF control was employed to attenuate quasi-periodic oscillations and the negative-sequence component caused by the symmetry breaking in an electric AC/AC conversion (Sánchez *et al.*, 2018). It was also employed to suppress complex pulses oscillations modes in modular multilevel converter of the high voltage DC transmission integration approach to large wind farms TDF control (Yu *et al.*, 2020). Tusset *et al.* (2021) treated atomic force microscopy, stabilizing a period-1 UPO of the chaotic state.

Chaos control takes advantages of its low energy consumption when stabilizing bi-stable cantilevers energy harvesters systems (De and Ali, 2022). In quantum theory, the visibility of two photons emitted from a three-level system could be enhanced significantly, boosting the energy-time entanglement using TDF control Barkemeyer *et al.* (2021). Regarding biomechanics, irregular and chaotic heartbeat behaviors can be suppressed using ETDF control on electrocardiograms signals (Ferreira *et al.*, 2014). ETDF control can provide stabilization of thermomechanical vibrations of shape memory alloy structures, showing its importance for the control of smart structures (Costa and Savi, 2018; Costa *et al.*, 2019).

This article aims to investigate a generalization of the Extended Time-Delayed Feedback control method, exploring its gain. Basically, the usual approach adopts a scalar gain. Here, a matrix gain is of concern. A case study of a nonlinear pendulum is of concern, allowing one to exploit all the potentialities of the proposed approach.

EXTENDED TIME-DELAYED FEEDBACK CONTROL

The ETDF control method proposed by Pyragas (1992) is based on a continuous-time perturbation to perform chaos control. This controller is applied to dynamical systems modeled by a set of equations with the following form:

$$\dot{x}(t) = f(x,t) + B(t) \tag{1}$$

where $x(t) \in R^n$ is the state variables, $f(x,t) \in R^n$ define the system dynamics and $B(t) \in R^n$ is associated with the control action.

The ETDF control is based on feedback of the difference between the current and a delayed states, and the perturbation is given by:

$$\begin{aligned} B(t) &= \mathbf{K}[(1-R)S_\tau - x] \\ S_\tau &= \sum_{m=1}^{\infty} R^{m-1} x_{m\tau} \end{aligned} \tag{2}$$

where τ is the time delay, $\mathbf{K} \in R^{n\times n}$ is the gain matrix, $0 \leq R < 1$ is a controller parameter related to higher orders time delays, $x = x(t)$ and $x_{m\tau} = x(t - m\tau)$. It should be noted that the use of the gain as a matrix $\mathbf{K}$ is a generalization of the method since the literature usually considers a scalar gain k_{nn}. It is worth noting that for $R = 0$ the equation falls into the TDFC method, where only a single delayed state is considered.

The UPO stabilization is achieved by choosing proper values of R and $\mathbf{K}$. Furthermore, when the system reaches a specific UPO, the Eq. 2 goes to zero since $y(t - m\tau) = y(t)$ for all m if $\tau = T_i$, where T_i is the periodicity of the ith UPO.

The controlled dynamical system, composed by Eqs. 1 and 2, is related to delay-differential equations (DDEs). The solution of this set of equations is done by establishing an initial function $y_0 = y_0(t)$ over the interval $(-m\tau, 0)$. This function can be estimated by a Taylor series expansion proposed by Cunningham (1954):

$$y_{m\tau} = y - m\tau\dot{y} \tag{3}$$

Therefore, the system is governed by:

$$\begin{aligned} \dot{x}(t) &= f(x,t) + \mathbf{K}[(1-R)S_\tau - x] \\ S_\tau &= \sum_{m=1}^{\infty} R^{m-1}[y - m\tau\dot{y}] \text{ for } (t - m\tau) < 0 \end{aligned} \tag{4}$$

Numerical simulations are carried out employing the fourth-order Runge-Kutta method with linear interpolation on delayed variables (Mensour and Longtin, 1998). During the learning stage, UPO identification is done by applying the close-return method (Auerbach *et al.*, 1987). Moreover, it is necessary to establish a proper value of controller parameters R and $\mathbf{K}$ for each desired UPO. This determination can be done by considering Lyapunov exponents of the corresponding UPO, which is discussed in the next subsection. After this stage, the control stage is performed where the desired UPO is stabilized.

UPO Lyapunov Exponent

Time-delayed feedback control is based on a construction of a continuous-time perturbation in such manner that does not change the desired UPO, but only its characteristics (Kittel *et al.*, 1994). This is achieved when such characteristics are modified to make the orbit stable. The Lyapunov exponent is a system invariant that measures the sensitivity to initial conditions by monitoring adjacent trajectories. A negative Lyapunov exponent means that nearby trajectories converge. Therefore, by changing controller parameters in order to force all Lyapunov exponents to become negative, leads to the stabilization of the UPO (Kittel *et al.*, 1995). Furthermore, only the largest Lyapunov exponent is enough to make this analysis (Pyragas, 1995). The strategy to define the controller parameters is to change the parameters R and $\mathbf{K}$, monitoring the maximum exponent and seeking for negative values. In other words, it is necessary to find a situation where $\lambda(R,\mathbf{K}) < 0$. The controller tends to be more effective, presenting faster convergence rate by considering the smaller Lyapunov exponent as possible (Pyragas, 1995). This condition also ensures robustness with respect to noise.

Lyapunov exponent computation from DDEs is more complicated than ODEs due to the dependence on delayed states. By considering three delayed states, the Eq. 1 becomes:

$$\dot{x} = f(x,t) + B(t, x, x_\tau, x_{2\tau}, x_{3\tau}) \tag{5}$$

Therefore, the calculation of $y = y(t)$ for time instants greater than τ implies that the function must be known over the interval $(t - 3s, t)$. This is related to an infinite-dimensional system with an infinite number of Lyapunov exponents

(Vicente *et al.*, 2005). Concerning the stability analysis of the UPO, it is enough to determine only the largest Lyapunov exponent (Pyragas, 1995).

In addition, just a finite dimension is considered (Farmer, 1982). Herewith, the function $x_i(t)$, with $i = 1,\ldots,n$, in the range $(t-3\tau,t)$ can be approximated by N samples of spacing $\Delta t = 3\tau/(N-1)$. Therefore, the system goes from n state variables to $(N+1)$ variables. A vector z is used to represent these state variables, where $z_{n+1},\ldots,z_{n(N+1)}$ are related to the time-phased states of $x(t)$ in the form:

$$(z_1,z_2,\ldots,z_{N+1}) = (x_1(t),x_2(t),\ldots,x_n(t),x_1(t-\Delta t),\ldots,x_1(t-N\Delta t),\ldots,x_n(t-\Delta t),\ldots,x_n(t-N\Delta t)) \tag{6}$$

In this work, the approach presented in Sprott (2007) is employed, where the DDE is replaced by a set of ODEs with the form:

$$\begin{cases} \dot{z}_j = f_j(z_1,z_2,\ldots,z_n) + B_j(t,z_1,\ldots,z_n,z_{n+1},\ldots,z_{n(N+1)}) & \text{para } 1 \le j \le n \\ \dot{z}_{n+1+(j-1)N} = N(z_j - z_{n+2+(j-1)N})/2\tau & \text{para } 1 \le j \le n \\ \dot{z}_{n+i+(j-1)N} = N(z_{n+i+(j-1)N-1} - z_{n+i+(j-1)N+1})/2\tau & \text{para } 2 \le i \le (N-1) \\ & \text{e } 1 \le j \le n \\ \dot{z}_{n+jN} = N(z_{n+jN-1} - z_{n+jN})/\tau & \text{para } 1 \le j \le n \end{cases} \tag{7}$$

where $N = 3\tau/\Delta t + 1$ and $T = 3\tau$. Therefore, this system can be solved by any of the standard integration methods such as the fourth- order Runge–Kutta, and Lyapunov exponents can be calculated by using the algorithm proposed Wolf *et al.* (1985).

NONLINEAR PENDULUM

As a mechanical application of the ETDF control method, a nonlinear pendulum, showed in Fig. 1, is considered (de Paula *et al.*, 2006). A mathematical model is developed to describe the pendulum dynamical behavior while the corresponding parameters are obtained from the experimental apparatus. Numerical simulations are employed to obtain time series related to the pendulum response assuming the uncontrolled situation, $K_{ij} = 0$ for all i, j and $R = 0$. Unstable periodic orbits are identified from this time series using the close-return method. Afterward, control parameters are estimated for each UPO from the calculation of the Lyapunov exponents and their control is then simulated via extended time-delayed feedback control.

The nonlinear pendulum consists of an aluminum disc (1) with a lumped mass (2) that is connected to a rotary motion sensor (4). A magnetic device (3) provides adjustable energy dissipation. A string–spring device (6) provides torsional stiffness to the pendulum and an electric motor (7) excites the pendulum via the string-spring device. An actuator (5) is considered to provide the necessary perturbations to stabilize this system.

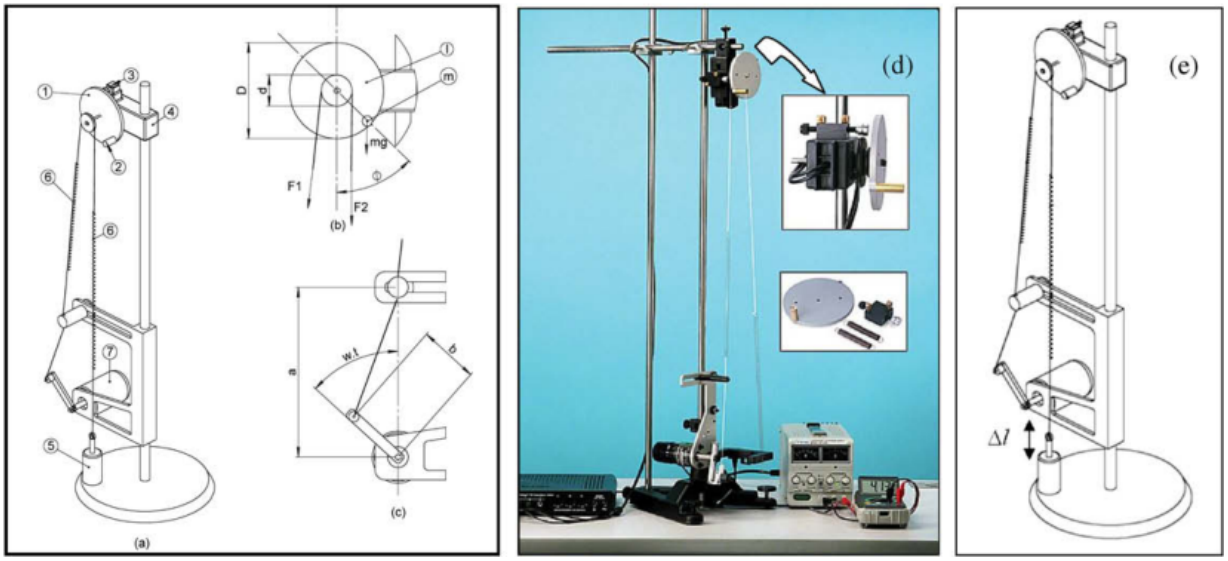

Figure 1: Nonlinear pendulum. (a) Physical model: (1) metallic disc; (2) lumped mass; (3) magnetic damping device; (4) rotary motion sensor; (5) actuator; (6) string–spring device; (7) electric motor. (b) Parameters and forces on the metallic disc; (c) parameters from driving device; (d) experimental apparatus; and (e) actuator.

The pendulum dynamics is treated from a mathematical model by describing the time evolution of the angular position, ϕ. By assuming that $\bar{\omega}$ is the forcing frequency, I is the total inertia of rotating parts, k is the spring stiffness, ζ represents the viscous damping coefficient and μ the dry friction coefficient, m is the lumped mass, a defines the position of the guide of the string with respect to the motor, b is the length of the excitation arm of the motor, D is the diameter of the metallic disc and d is the diameter of the driving pulley, the equation of motion is given by Eq. 8

$$\ddot{\phi} + \frac{\zeta}{I}\dot{\phi} + \frac{\mu\,\mathrm{sgn}(\dot{\phi})}{I} + \frac{kd^2}{2I}\phi + \frac{mgD\sin(\phi)}{2I} = \Delta f(t) \tag{8}$$

where $\Delta f(t) = \frac{kd}{2I}\left[\sqrt{a^2+b^2-2ab\cos(\bar{\omega}t)} - (a-b)\right]$ represents the forcing excitation.

The dry friction is modeled as a continuous function by assuming $\mu\,\mathrm{sgn}(\dot{\phi}) = \frac{2}{\pi}\mu\arctan(q\cdot\dot{\phi})$.Rewriting the equation of motion in the form of a system of first-order ordinary differential equations as a function of the state variables $(x_1, x_2) = (\phi, \dot{\phi})$ and adding the controller action **B**:

$$\begin{Bmatrix} \dot{x_1} \\ \dot{x_2} \end{Bmatrix} = \begin{bmatrix} 0 & 1 \\ -\frac{kd^2}{2I} & -\frac{\zeta}{I} \end{bmatrix} \begin{Bmatrix} x_1 \\ x_2 \end{Bmatrix} + \begin{Bmatrix} B_1(t) \\ \frac{kd}{2I}\Delta f(t) - \frac{mgD}{2I}\sin(x_1) - \frac{2\mu}{I\pi}\arctan(qx_2) + B_2(t) \end{Bmatrix} \tag{9}$$

where the controller actuation is given by:

$$\mathbf{B}(t) = \begin{Bmatrix} B_1(t) \\ B_2(t) \end{Bmatrix} = \begin{bmatrix} k_{11} & k_{12} \\ k_{21} & k_{22} \end{bmatrix} \begin{Bmatrix} (1-R)S_{\tau 1} - x_1 \\ (1-R)S_{\tau 2} - x_2 \end{Bmatrix} \tag{10}$$

It is assumed the same parameters presented for all numerical simulations: $a = 1.6\times10^{-1}$ m; $b = 6.0\times10^{-2}$ m; $d = 4.8\times10^{-2}$ m; $D = 9.5\times10^{-2}$ m; $m = 1.47\times10^{-2}$ kg; $I = 1.738\times10^{-4}$ kg m^2; $k = 2.47$ N/m; $\zeta = 2.368\times10^{-5}$ kg m^2 s^{-1}; $mu = 1.272\times10^{-4}$ Nm; $\omega = 5.61$ rad/s.

Usually, the literature brings the formulation where the controller acts as a torque. In this regard, the gain matrix **K** is reduced to a scalar, being represented as follows:

$$\mathbf{K} = \begin{bmatrix} K_{11} & K_{12} \\ K_{21} & K_{22} \end{bmatrix} = \begin{bmatrix} 0 & 0 \\ 0 & K_{22} \end{bmatrix} = \begin{bmatrix} 0 & 0 \\ 0 & K \end{bmatrix} \tag{11}$$

Which means that $B_1 = 0$ and $B_2 = -\frac{kd}{2I}\Delta l(t)$. The perturbations are provided by the linear actuator which represents a variation in the length of the string $\Delta l(t)$ (see Fig. 1(e) for details). Thus, from Eq. 10 can write the value of $\Delta l(t)$ as:

$$-\frac{kd}{2I}\Delta l = K[(1-R)S_{\tau 2} - x_2] \tag{12}$$

This work proposes the full gain matrix **K**. The first line of the state function measures angular speed and the second one measures angular acceleration. On this basis, the control can be evaluated for both states independently. From Eq. 10:

$$\begin{Bmatrix} B_1(t) \\ B_2(t) \end{Bmatrix} = \begin{Bmatrix} K_{11}[(1-R)S_{\tau 1} - x_1] + K_{12}[(1-R)S_{\tau 2} - x_2] \\ K_{21}[(1-R)S_{\tau 1} - x_1] + K_{22}[(1-R)S_{\tau 2} - x_2] \end{Bmatrix} \tag{13}$$

The term B_1 is related to angular velocity of the system. On the other hand, the control action for B_2 is given by:

$$B_2 = -\frac{kd}{2I}\Delta l = K_{21}[(1-R)S_{1\tau} - x_1] + K_{22}[(1-R)S_{2\tau} - x_2] \tag{14}$$

where $S_{i\tau} = x_i(t-\tau) + Rx_i(t-\tau) + R^2x_i(t-\tau)$ com $i = 1, 2$.

LEARNING STAGE

The first step of the chaos control is the learning stage where UPO are identified and the gains are determined from the Lyapunov exponents of each UPO.

The system attractor has a infinity number of UPOs and their identification are found using the close returning points method (Auerbach *et al.*, 1987) with a tolerance of $r_1 = 0.01$. Different UPOs are selected and presented in in Figure 3: period-1, period-2 and period-3.

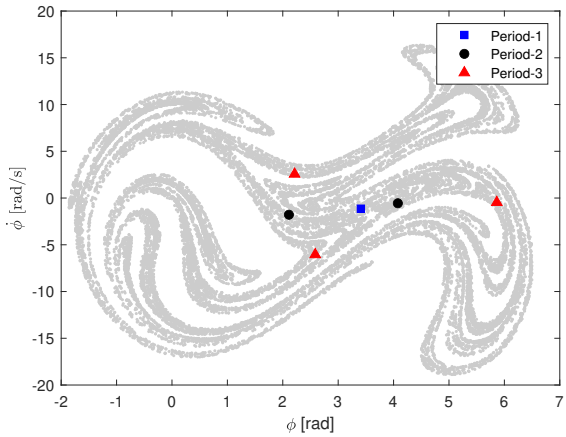

Figure 2: UPOs of the control rule;
■: period-1, ●: period-2, ▲: period-3.

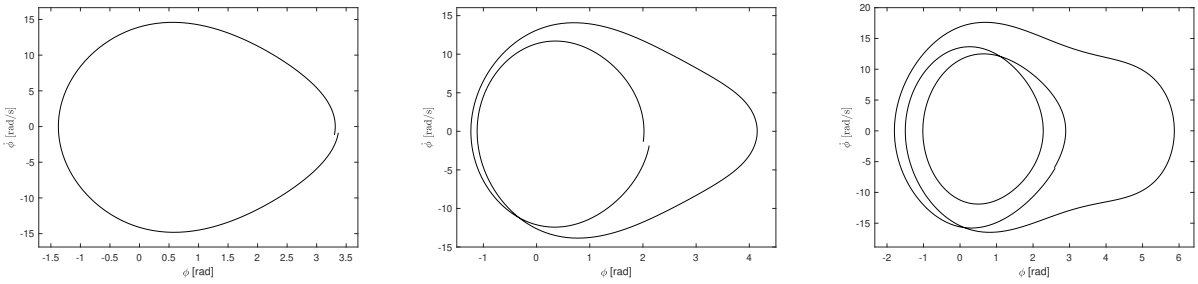

(a) UPO period-1; (b) UPO period-2; (c) UPO period-3;

Figure 3: UPOs of the control rule.

The second phase of the learning stage evaluates the gains from the Lyapunov exponent analysis. This is the most computationally expensive control phase. Table 1 presents Lyapunov exponent for each selected UPO without control, showing its unstable characteristic from the positive values.

Table 1: Lyapunov exponent for selected UPOs without control.

Period	Lyapunov Exponent
1	1.531
2	1.411
3	0.638

To verify the ETDF method capacity to perform the stabilization of an UPO, numerical simulation of the nonlinear pendulum is performed, varying controller parameters. The evaluation is performed for values of $R = 0.0$, $R = 0.2$ and $R = 0.4$. Different aspects of the matrix $\mathbf{K}$ are of concern. The K_{21} and K_{22} values are varied from 0 to 2.5 with an interval of 0.2. The same process is repeated for K_{11} and K_{12}, and K_{11} and K_{22} values.

Higher periodicity UPOs tend to have more difficult stabilization, requiring greater values of R to reach negative Lyapunov exponents (de Paula and Savi, 2009). The choice of the gains R and $\mathbf{K}$ are performed by the lowest Lyapunov exponents. The minimum value of the exponent provides a higher rate of convergence of nearby orbits (Pyragas, 1995). Smaller values of R and $\mathbf{K}$ implies in a less modified system, which is a desirable situation.

Figure 4 presents the maximum Lyapunov exponent for period-1 UPO. Sub-figure 4a refers to Lyapunov exponent considering a scalar K for $R = 0.0$, $R = 0.2$, $R = 0.4$, as showed in the literature (de Paula and Savi, 2009; De Paula and Savi, 2011). Sub-figure 4b incorporates parameters K_{11} and K_{12} in the analysis. The influence of parameter K_{11}, showed in Figures 4e and 4f, are related to a larger area of the negative Lyapunov exponent. The magnitudes are similar

when comparing to scalar K. Sub-figures 4c and 4d indicate Lyapunov exponent considering both K_{21} and K_{22} for $R = 0.0$, $R = 0.2$ respectively. The Lyapunov exponents in Figures 4c and 4d showed a great influence of the parameter K_{21} resulting in larger area of negative exponents when compared to the use of K_{22} only. The maximum values of the Lyapunov exponent considering the two parameters K_{21} and K_{22} have magnitudes close to the case of scalar K . This result is valid for the three R values analyzed.

Figure 5 presents the Lyapunov exponents for period-2 UPO. Figure 5a considers only a scalar K, showing negative values for $R = 0.2$ and $R = 0.4$. Similarly, it does not show negative Lyapunov exponent regions by considering K_{21} and K_{22} for $R = 0.0$. Sub-figure 5b refers to Lyapunov exponent considering both K_{21} and K_{22} for $R = 0.2$. The selection of the gain values K_{21} and K_{22} shows maximum Lyapunov exponent values on the same magnitude than those considering a scalar gain K. For $R = 0.2$, there is a small influence of the parameter K_{21} regarding the negative exponent area. Unlike the period-1 UPO, smaller exponents are obtained for this UPO by using 2 parameters in he matrix gain $\mathbf{K}$ with respect to a scalar gain K. Sub-figure 5c considers Lyapunov exponent evaluating both K_{11} and K_{22} for $R = 0.4$ It shows an increase in the area of negative Lyapunov exponents when compared to K_{21} and K_{22}. It also shows smaller Lyapunov exponent values compared with the case with scalar gain K.

Figure 6 considers period-3 UPO. Figure 6 shows a small area for negative Lyapunov exponent by considering a scalar gain K, increasing the area by considering both K_{21} and K_{22} for the three values of R, and presenting smaller values of the maximum Lyapunov exponent.

The selected Lyapunov exponent considering a scalar K and for matrix $\mathbf{K}$ are shown in Table 2, 3 respectively.

Table 2: Lyapunov Exponent selected for a scalar K.

Period	R	K_{22}	Lyapunov Exponent
1	0.0	1.9	-0.448
2	0.2	1.2	-0.108
3	0.2	0.6	-0.198

Table 3: Lyapunov Exponent selected for $\mathbf{K}$ matrix.

Period	R	K_{11}	K_{21}	K_{22}	Lyapunov Exponent
1	0.2	0.0	0.1	2.4	-0.445
1	0.0	0.2	0.0	1.4	-0.448
2	0.2	0.0	1.1	1.2	-0.158
3	0.2	0.0	0.2	0.6	-0.203

STABILIZATION STAGE

The stabilization stage is now of concern considering simulations during 100 forcing cycles. The equations are solved using the fourth-order Runge-Kuta method with a discretization of 150 units per cycle. The initial conditions are null.

The controller performance is evaluated by considering the following criteria: it is evaluated whether the UPO is stabilized; the time required to stabilize the UPO. The stabilization time is evaluated by considering the Euclidean distance between $\dot{\phi}$ and $\ddot{\phi}$ of the reference orbits and the controlled orbit. A threshold of the Euclidean distance is stimulated, being 1 for a period-1 UPO and 3 for period-2 and period-3 UPOs. Each case is treated considering phase spaces after 50 cycles compared with the desired UPO, time history of the response and the control signal.

This work compares different controller defined from the gain. The reference case is the classical scalar gain $K = K_{22}$, usually employed in the literature (de Paula and Savi, 2009; De Paula and Savi, 2011). Matrix gain $\mathbf{K}$ considers two different situations: using both K_{21} and K_{22} where only B_2 action occurs; using both K_{11} and K_{22} which means that the action has both B_1 and B_2.

Stabilization of period-1 UPO by considering controllers with scalar gain K and K_{21} and K_{22}, is shown in Figures 8. Note that a shorter time occurs when using K_{21} and K_{22} compared with the scalar gain. The stabilization with $\mathbf{K}$ presents a maximum actuation value of $\Delta l = 154.7$ mm while for the scalar gain K presents $\Delta l = 129.4$ mm. By considering both gain parameters, it is possible to stabilize the system in a similar time using a smaller maximum actuation of $\Delta l = 127.6$ mm. Some other combinations of K_{21} and K_{22} are able to stabilize the pendulum within less time or with an smaller actuation than considering only the scalar gain, therefore it increases possible control gain choices bringing more flexibility to the controller.

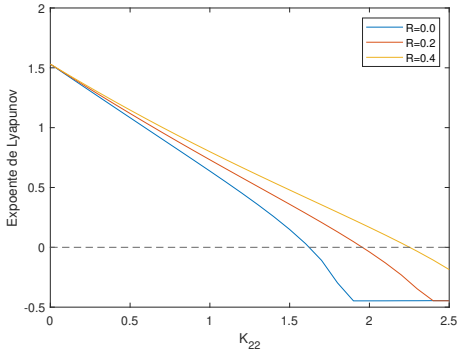

(a) Scalar K with multiple R.

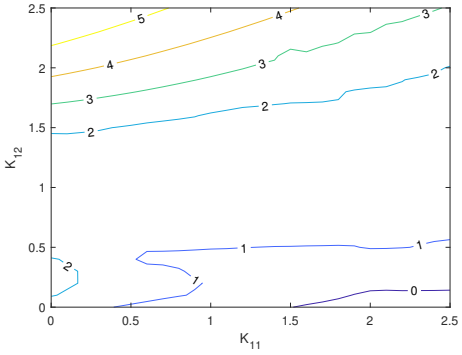

(b) K_{11} and K_{12} for $R = 0.0$.

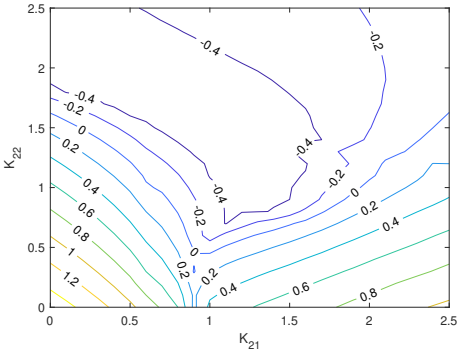

(c) K_{21} and K_{22} for $R = 0.0$.

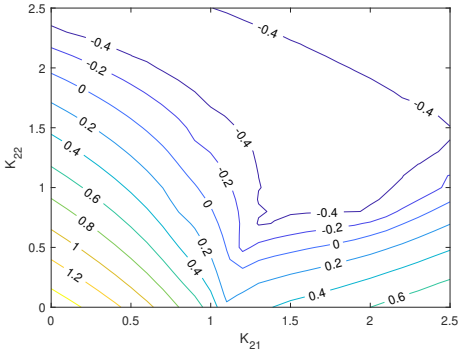

(d) K_{21} and K_{22} for $R = 0.2$.

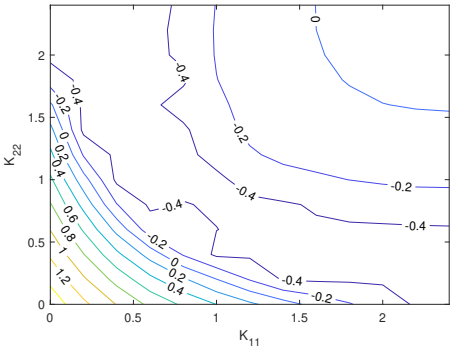

(e) K_{11} and K_{22} for $R = 0.0$.

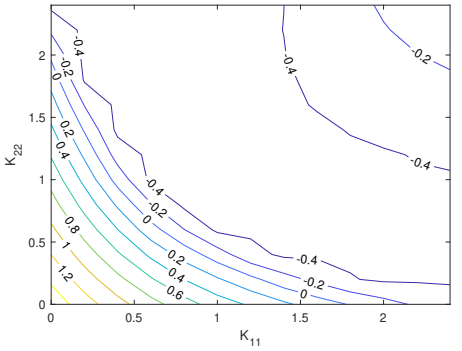

(f) K_{11} and K_{22} for $R = 0.2$.

Figure 4: Period-1 UPO and the largest Lyapunov exponent for different control parameters.

The controller that employs the gains K_{11} and K_{22} is presented in Figure 8, comparing with the scalar gain K. Figure 8a shows a comparison of phase space, while Figure 8b shows time history of control signal for a scalar gain K and for each B_1 and B_2 control signals for both K_{11} and K_{22}. Control using both K_{11} and K_{22} gains, the stabilization is achieved in a similar time. Maximum actuator length for B_2 is $\Delta l = 96.9$ mm, about 75% of Δl by considering a scalar gain K.

Stabilization is achieved in similar time lengths when comparing the influence of parameter K_{11} with K_{21}. The actuator maximum length was 25% smaller when the controllergain K_{11} is considered.

Figure 9 presents the stabilization of the the period-2 UPO. Although the control signal is bigger, the system can stabilize the UPO in a faster way.

Period-3 UPO control is now in focus. Figure 10 shows the controller action and, similarly to period-1 UPO, it is possible to stabilize the period-3 UPO within a smaller time when using both controller gains K_{21} and K_{22} than by considering the scalar gain K. Although the maximum actuator lengths are similar, $\Delta l = 40.6$ mm for only K and $\Delta l = 40.5$ mm for both K_{21} and K_{22}.

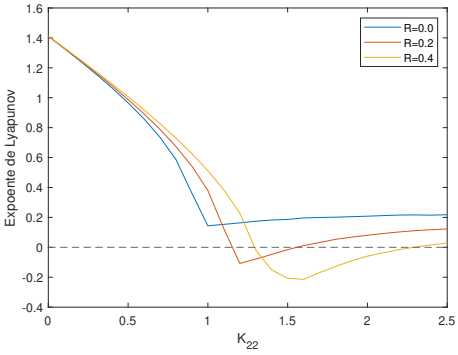

(a) Scalar K with multiple R.

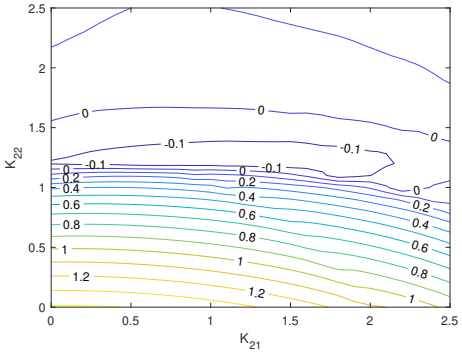

(b) K_{21} and K_{22} for $R = 0.2$.

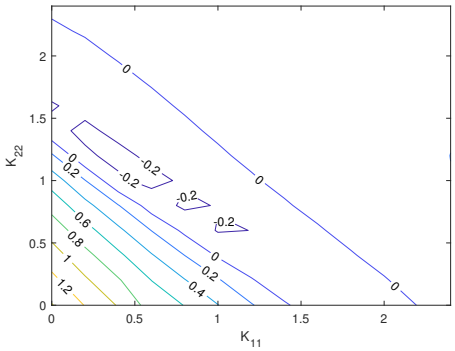

(c) K_{11} and K_{22} for $R = 0.4$.

Figure 5: Period-2 UPO and the largest Lyapunov exponent for different control parameters.

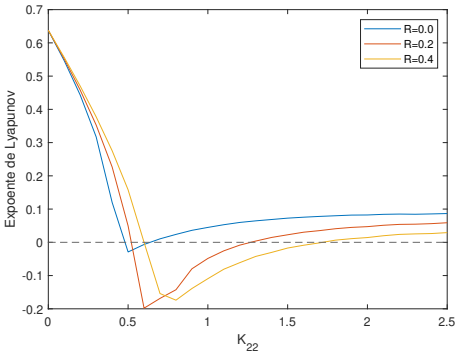

(a) Scalar K with multiple R.

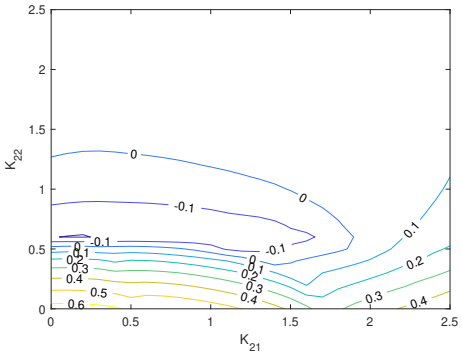

(b) K_{21} and K_{22} for $R = 0.2$.

Figure 6: Period-3 UPO and the largest Lyapunov exponent for different control parameters.

Table 4 shows the maximum Δl of actuator of the controller with a scalar gain K while Table 5 shows the same information using the controller with matrix $\mathbf{K}$.

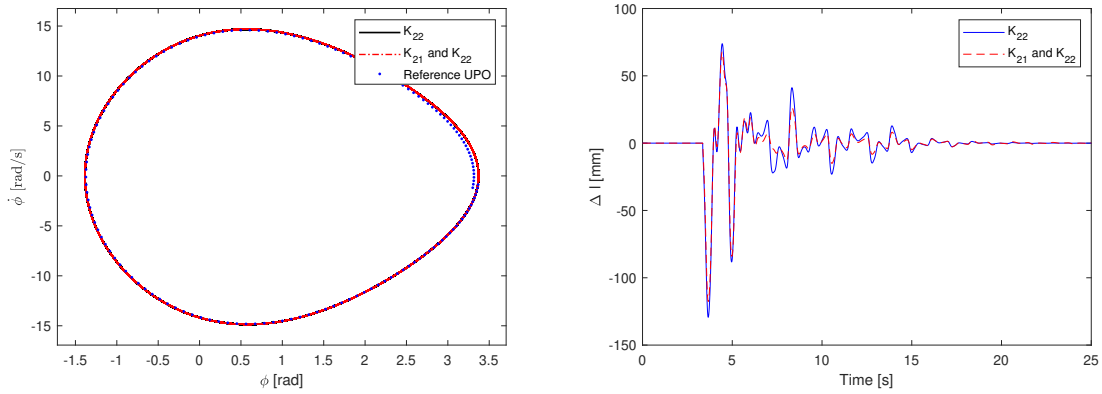

(a) Phase Space of reference and controlled.

(b) Control signal in time.

Figure 7: Control comparison for only K_{22} and with both K_{21} and K_{22} for period-1 UPO.

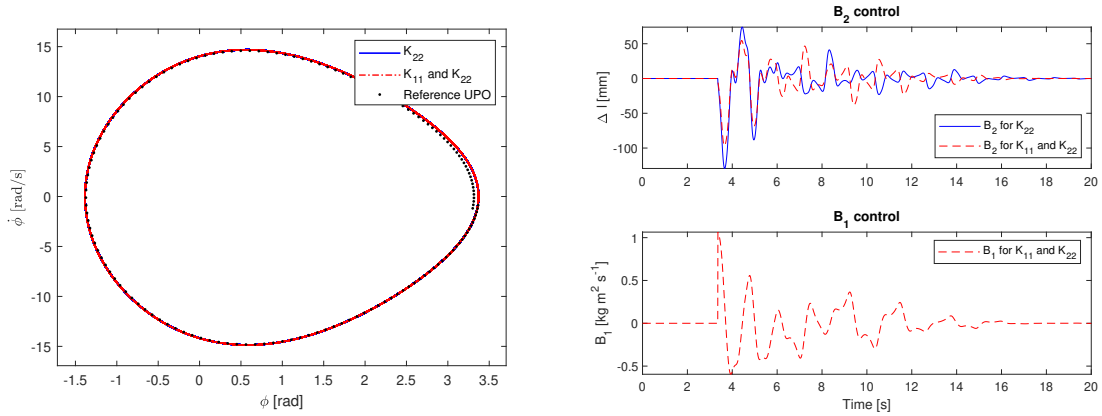

(a) Phase Space of reference and controlled.

(b) Control signal in time.

Figure 8: Control comparison for only K_{22} and with both K_{11} and K_{22} for period-1 UPO.

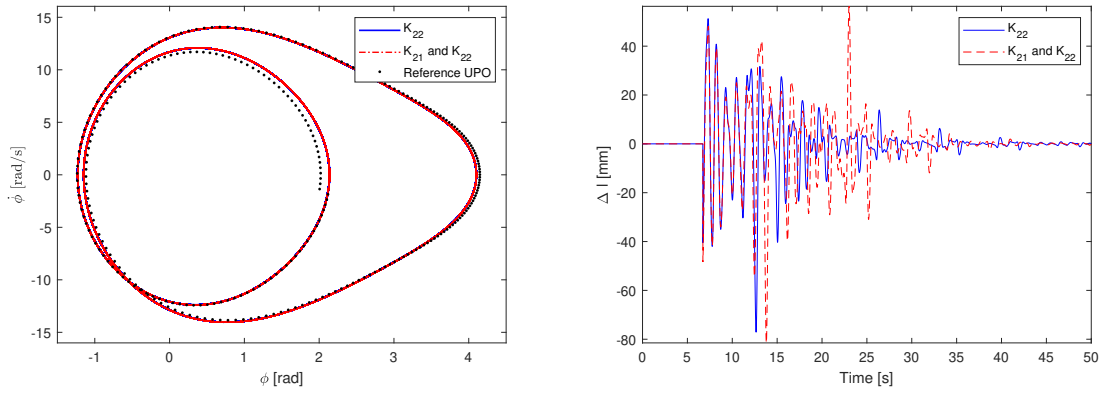

(a) Phase Space of reference and controlled.

(b) Control signal in time.

Figure 9: Control comparison for only K_{22} with both K_{21} and K_{22} for period-2 UPO.

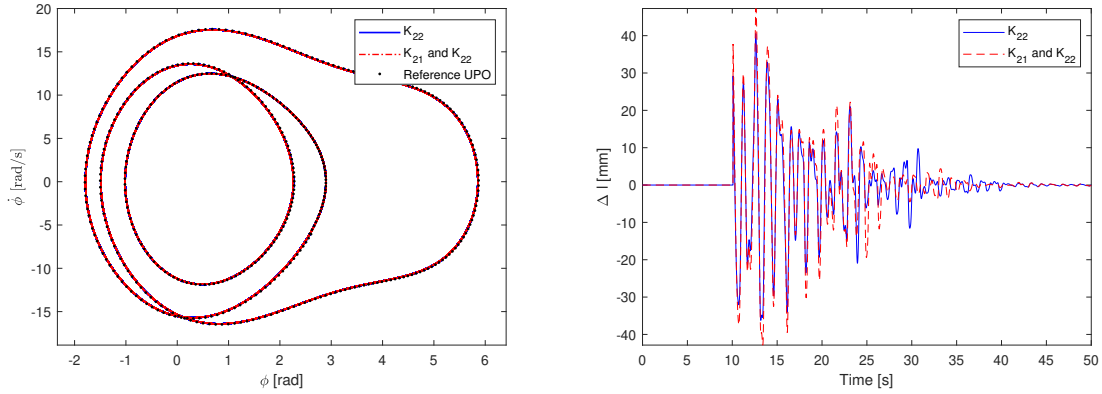

(a) Phase Space of reference and controlled.

(b) Control signal in time.

Figure 10: Control comparison for only K_{22} with both K_{21} and K_{22} for period-3 UPO.

Table 4: Maximum actuation using a scalar K.

Period	R	K_{21}	Lyapunov Exponent	Δl_{max} [mm]
1	0.0	1.9	-0.448	129.4
2	0.2	1.2	-0.108	77.1
3	0.2	0.6	-0.198	40.6

Table 5: Maximum actuation in the controller using **K**.

Period	R	K_{11}	K_{21}	K_{21}	Lyapunov Exponent	Δl_{max} [mm]
1	0.0	0.0	0.2	1.7	-0.284	117.6
1	0.0	0.0	0.1	1.8	-0.413	123.5
1	0.2	0.0	0.1	2.4	-0.445	154.7
1	0.0	0.2	0.0	1.4	-0.448	96.9
1	0.0	0.2	0.0	1.6	-0.448	119.6
1	0.0	0.2	0.2	1.4	-0.442	96.5
2	0.2	0.0	0.7	1.2	-0.152	81.5
2	0.2	0.0	1.6	1.1	-0.169	76.5
3	0.2	0.0	0.3	0.6	-0.197	40.5
3	0.2	0.0	0.2	0.6	-0.203	40.5

CONCLUSIONS

This paper presents a generalization of the extended time-delayed feedback (ETDF) control method with a matrix **K** gain, establishing a comparison with the classical scalar gain. The control method is applied to a nonlinear pendulum in order to stabilize some UPOs embedded in the chaotic attractor. The learning stage is developed by identifying UPOs and employing the maximum Lyapunov exponent to define controller parameters. The search for Lyapunov exponents using the parameters K_{21} and K_{22} or K_{11} and K_{22} revealed a larger region of negative values for the exponent when compared with the case with a scalar gain K. Lower maximum values are observed in UPOs of period-2 and period-3 evaluated when considering 2 controller gains. Moreover, there is a larger area of negative Lyapunov exponent increasing the number of possibilities for successfully control, therefore making it more versatile. Regarding the stabilization stage using both K_{21} and K_{22}, it is able to choose controller gains that reduce maximum actuation and time to stabilize. The stabilization using K_{11} and K_{22} can be achieved in smaller times. Therefore, the use of the generalized ETDF with controller gains associated with its matrix form brings great flexibility to the system, defining a controller with best efficacy than the original one.

ACKNOWLEDGMENTS

The authors would like to acknowledge the support of the Brazilian Research Councils CNPq, CAPES and FAPERJ.

REFERENCES

Auerbach, D., Cvitanović, P., Eckmann, J.P., Gunaratne, G. and Procaccia, I., 1987. "Exploring chaotic motion through periodic orbits". *Physical Review Letters*, Vol. 58, No. 23, p. 2387.

Barkemeyer, K., Hohn, M., Reitzenstein, S. and Carmele, A., 2021. "Boosting energy-time entanglement using coherent time-delayed feedback". *Physical Review A*, Vol. 103, No. 6, p. 062423.

Costa, D.D. and Savi, M.A., 2018. "Chaos control of an sma–pendulum system using thermal actuation with extended time-delayed feedback approach". *Nonlinear Dynamics*, Vol. 93, No. 2, pp. 571–583.

Costa, D.D., Savi, M.A., de Paula, A.S. and Bernardini, D., 2019. "Chaos control of a shape memory alloy structure using thermal constrained actuation". *International Journal of Non-Linear Mechanics*, Vol. 111, pp. 106–118.

Cunningham, W.J., 1954. "A nonlinear differential-difference equation of growth". *Proceedings of the National Academy of Sciences of the United States of America*, Vol. 40, No. 8, p. 708.

De, S.L. and Ali, S.F., 2022. "Dynamics of bi-stable energy harvesters with delayed feedback control". *IFAC-PapersOnLine*, Vol. 55, No. 1, pp. 411–416.

de Paula, A.S. and Savi, M.A., 2009. "Controlling chaos in a nonlinear pendulum using an extended time-delayed feedback control method". *Chaos, Solitons & Fractals*, Vol. 42, No. 5, pp. 2981–2988.

De Paula, A.S. and Savi, M.A., 2011. "Comparative analysis of chaos control methods: A mechanical system case study". *International Journal of Non-Linear Mechanics*, Vol. 46, No. 8, pp. 1076–1089.

de Paula, A.S., Savi, M.A. and Pereira-Pinto, F.H.I., 2006. "Chaos and transient chaos in an experimental nonlinear pendulum". *Journal of sound and vibration*, Vol. 294, No. 3, pp. 585–595.

Farmer, J.D., 1982. "Chaotic attractors of an infinite-dimensional dynamical system". *Physica D: Nonlinear Phenomena*, Vol. 4, No. 3, pp. 366–393.

Ferreira, B.B., Savi, M.A. and de Paula, A.S., 2014. "Chaos control applied to cardiac rhythms represented by ecg signals". *Physica Scripta*, Vol. 89, No. 10, p. 105203.

Gjurchinovski, A., Jüngling, T., Urumov, V. and Schöll, E., 2013. "Delayed feedback control of unstable steady states with high-frequency modulation of the delay". *Physical Review E*, Vol. 88, No. 3, p. 032912.

Jüngling, T., Gjurchinovski, A. and Urumov, V., 2012. "Experimental time-delayed feedback control with variable and distributed delays". *Physical Review E*, Vol. 86, No. 4, p. 046213.

Kittel, A., Pyragas, K. and Richter, R., 1994. "Prerecorded history of a system as an experimental tool to control chaos". *Physical Review E*, Vol. 50, No. 1, p. 262.

Kittel, A., Parisi, J. and Pyragas, K., 1995. "Delayed feedback control of chaos by self-adapted delay time". *Physics Letters A*, Vol. 198, No. 5-6, pp. 433–436.

Mensour, B. and Longtin, A., 1998. "Power spectra and dynamical invariants for delay-differential and difference equations". *Physica D: Nonlinear Phenomena*, Vol. 113, No. 1, pp. 1–25.

Ott, E., Grebogi, C. and Yorke, J.A., 1990. "Controlling chaos". *Physical review letters*, Vol. 64, No. 11, p. 1196.

Pyragas, K., 1992. "Continuous control of chaos by self-controlling feedback". *Physics letters A*, Vol. 170, No. 6, pp. 421–428.

Pyragas, K., 1995. "Control of chaos via extended delay feedback". *Physics letters A*, Vol. 206, No. 5-6, pp. 323–330.

Pyragas, V. and Pyragas, K., 2011. "Adaptive modification of the delayed feedback control algorithm with a continuously varying time delay". *Physics letters A*, Vol. 375, No. 44, pp. 3866–3871.

Pyragas, V. and Pyragas, K., 2013. "Adaptive search for the optimal feedback gain of time-delayed feedback controlled systems in the presence of noise". *The European Physical Journal B*, Vol. 86, No. 7, pp. 1–8.

Sánchez, M., Okuda, T. and Hikihara, T., 2018. "Stabilization of mode in imbalanced operation of matrix converter by time-delayed feedback control". *International Journal of Circuit Theory and Applications*, Vol. 46, No. 12, pp. 2420–2433.

Selivanov, A., Lehnert, J., Fradkov, A. and Schöll, E., 2015. "Adaptive time-delayed stabilization of steady states and periodic orbits". *Physical Review E*, Vol. 91, No. 1, p. 012906.

Socolar, J.E., Sukow, D.W. and Gauthier, D.J., 1994. "Stabilizing unstable periodic orbits in fast dynamical systems". *Physical Review E*, Vol. 50, No. 4, p. 3245.

Sprott, J., 2007. "A simple chaotic delay differential equation". *Physics Letters A*, Vol. 366, No. 4-5, pp. 397–402.

Tusset, A.M., Balthazar, J.M., Ribeiro, M.A., Lenz, W.B. and Rocha, R.T., 2021. "Chaos control of an atomic force microscopy model in fractional-order". *The European Physical Journal Special Topics*, Vol. 230, No. 18, pp. 3643–3654.

Vicente, R., Daudén, J., Colet, P. and Toral, R., 2005. "Analysis and characterization of the hyperchaos generated by a semiconductor laser subject to a delayed feedback loop". *IEEE Journal of Quantum Electronics*, Vol. 41, No. 4, pp. 541–548.

Wolf, A., Swift, J.B., Swinney, H.L. and Vastano, J.A., 1985. "Determining lyapunov exponents from a time series". *Physica D: Nonlinear Phenomena*, Vol. 16, No. 3, pp. 285–317.

Yu, Y., Cheng, X., Zhang, C. and Ji, X., 2020. "Oscillation mechanism and mitigation of mmc-hvdc based on bifurcation theory for wind farm integration". *IEEE Access*, Vol. 8, pp. 125121–125129.

RESPONSIBILITY NOTICE

The author(s) is (are) the only responsible for the printed material included in this paper.